Photodissociation of hydrogen iodide in the A-band region 273–288 nm

Sergei Manzhos and Hans-Peter Loock[a)]
Department of Chemistry, Chernoff Hall, Queen's University, Kingston, ON, K7L 3N6, Canada

Bernard L. G. Bakker and David H. Parker
Department of Molecular and Laser Physics, University of Nijmegen, Nijmegen, P.O. Box 9010, NL-6500 GL, The Netherlands

(Received 25 June 2002; accepted 20 August 2002)

The photodissociation of hydrogen iodide in the A-band region was investigated between 273 and 288 nm using the photofragment imaging technique. At 17 wavelengths the I^* ($^2P_{1/2}$)/I($^2P_{3/2}$) branching ratio was measured by recording the corresponding hydrogen atomic fragment using multiphoton ionization at 243 nm. The branching ratios are in good agreement with previous measurements and confirm that four (final) states $^3\Pi(0^+)$, $^3\Pi(1)$, $^3\Sigma(1)$, and $^1\Pi(1)$ are involved in the A-band absorption of HI and that those states dissociate adiabatically to form H+I* and H+I following parallel and perpendicular transitions, respectively. The deficiency of the model of three unbound states and that of the δ-approximation is substantiated. © *2002 American Institute of Physics.* [DOI: 10.1063/1.1513250]

I. INTRODUCTION

Three to four electronic states of hydrogen iodide are responsible for the continuous absorption spectrum in the A-band between 180 and 280 nm. The band was first described by Mulliken,[1] who assigned the absorption to contributions of only one parallel $^3\Pi(0^+)\leftarrow X\,^1\Sigma(0^+)$ transition and two perpendicular transitions, i.e., $^3\Pi(1)\leftarrow X\,^1\Sigma(0^+)$ and $^1\Pi(1)\leftarrow X\,^1\Sigma(0^+)$. Mulliken also predicted that dissociation via the $^3\Pi(0^+)$ state would yield spin–orbit excited iodine atoms H(^{2}S)+I*($^2P_{1/2}$), whereas the dissociation of the $^1\Pi(1)$ and $^3\Pi(1)$ states would result in the formation of ground state iodine atoms H(^{2}S+I(^{2}P$_{3/2}$). In the following, the common notation for the iodine spin–orbit states, I(^{2}P$_{3/2}$)=I and I(^{2}P$_{1/2}$)=I*, will be adopted.

A lack of nonadiabatic interaction between these states was demonstrated in more recent studies[2,3] and allows for direct reconstruction of the partial absorption cross sections from the I*/I branching ratios. This analysis is aided by the distinct signature of the I* and I channels as expressed by the different spatial anisotropy of the photofragments. The two perpendicular H+I channels yield a spatial anisotropy parameter near its limiting value of $\beta=-1$; similarly the parallel transitions leading to H+I* yield $\beta=+2$.[2,3]

In this report we will argue that the contributions of a fourth state to the total absorption cross section cannot be neglected. The repulsive $t\ ^3\Sigma(1)$ state is accessed in a perpendicular transition leading to the photofragments' spatial anisotropy parameter near its limiting value of $\beta=-1$ and produces spin–orbit excited iodine atoms, i.e., H+I*. In the past years two research groups have conducted one-photon dissociation experiments of HI via the A-band. A study by Gendron and Hepburn (GH)[3] provided improved partial absorption cross sections for the three most prominent states of the A-band, the $^3\Pi(1)$, $^3\Pi(0^+)$, and $^3\Pi(1)$ states. Absorption of the $t\,^3\Sigma(1)$ state was assumed to be negligible. Earlier, branching ratios were published by Langford *et al.* (thereafter abbreviated to LROA).[4] Both groups measured the branching ratios over the whole width of the absorption spectrum but obtained different values. The I*/I data obtained by LROA using the hydrogen atom Rydberg tagging method were about 50% higher than the I*/I ratios obtained by GH using Doppler LIF spectroscopy at the Lyman-α transition of the H-atomic fragments. This controversy was more recently resolved by Regan *et al.* (RACAO),[5] who reexamined the branching ratios at five photolysis wavelengths using REMPI line intensities of the I and I* photofragment and found good agreement with GH. They also explained the deviation of the data by LROA as arising from an artifact in their analysis procedure due to a too-narrow bandwidth of the Lyman-α excitation laser. After a systematic correction of the data by LROA there now exists agreement between LROA and GH to within 20%, i.e., the experimental error of the measurements.

In this study, the long wavelength tail of the absorption spectrum, which was largely omitted from Gendron and Hepburn's study, was studied using yet another method. Photofragment imaging by the velocity map imaging technique[6] of the hydrogen atoms very reliably produces iodine branching ratios since the ratio between the H+I channel and H+I* channel is derived solely from the difference in the intensity of the corresponding hydrogen-fragment signal. Velocity mapping has the same potential pitfalls as the abovementioned Rydberg tagging studies of H atoms with respect to its sensitivity to the probe laser bandwidth. By using REMPI detection at 243 nm, however, the laser wavelength is more easily scanned across the transition profile, and any mismatch of the laser bandwidth and the Doppler width of the H atom transition is immediately obvious in the acquired im-

a)Author to whom correspondence should be addressed. Telephone (613) 533-2621, Fax: (613) 533-6669, Electronic mail: hploock@chem.queensu.ca

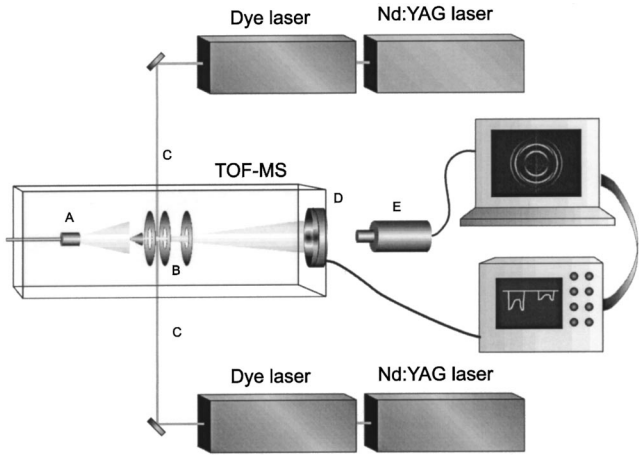

FIG. 1. Schematic diagram of the photofragment imaging apparatus in Nijmegen. Shown are the pulsed molecular beam valve "A," the three electrode assembly "B," the photolysis and ionization laser pulses "C," the position sensitive detector "D," and the camera with which the photofragment image is recorded "E."

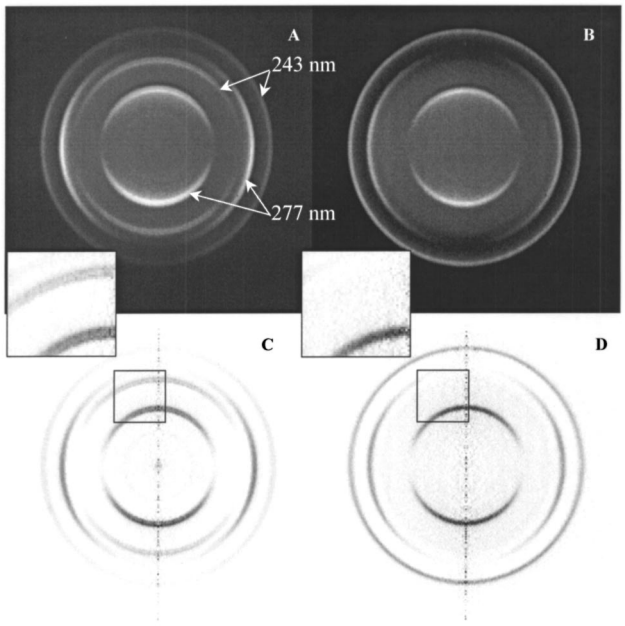

FIG. 2. H-atom photofragment image following excitation at 277 nm and ionization at 243.17 nm at vertical (A,C) and horizontal (B,D) polarization of the probe laser. The lower panels (C and D) show the inverse Abel transform of the raw image shown above. The splitting of the H-atom signal from the parallel H+I* channel only appears when the polarization of the probe laser is perpendicular to the TOF axis (see insets).

age. With this work we intend to provide additional data for the A-band branching ratios. In contrast to most earlier studies we focus on the long wavelength region of the A-band absorption spectrum. The data will be instrumental in the calculation of improved partial absorption cross sections (PACS) for the four states contributing to the A-band absorption. While we will use the additional data to demonstrate that four, and not three, states contribute to the A-band absorption, a detailed analysis is left to a parallel paper by Le Roy and co-workers.[7] In that paper it will then be shown that these PACS can be best fitted using three exponential functions and one Morse potential as potential energy curves for the states.

EXPERIMENTAL AND RESULTS

In our experiments hydrogen iodide (5% in 760 Torr Helium) is cooled in a supersonic expansion and excited by the frequency doubled output of a dye laser (Fig. 1). This photolysis laser is linearly polarized with both the direction of propagation and the electric field component perpendicular to the molecular beam. The hydrogen atomic fragment is detected via its REMPI line at 243.17 nm using the output of a second, similar laser system and a position sensitive ion detector. Since the Doppler width of the H-atom is wider than the probe laser linewidth, the laser had to be scanned over the absorption line while acquiring the image. The photofragment spectrometer in Nijmegen and the analysis technique are described in more detail elsewhere.[8] A typical image taken at an excitation wavelength of 277 nm is shown in Fig. 2. Between 1 and 4 measurements were taken at each of the 17 wavelengths between 273 and 288 nm and the branching ratio was derived from a Gaussian fit to the velocity distribution of the hydrogen atoms. This velocity distribution was obtained by integrating radially the pixels of the inverse Abel-transform of the ion image (Fig. 2). Since the probe laser at 243.17 nm is also able to dissociate the HI molecule, a second set of I and I* signals with higher kinetic energy release is always observed together with the pump and probe signal. It was possible to somewhat suppress the contribution of this signal by increasing the intensity and beam waist of the pump laser and thereby bleaching the molecular beam sample. Yet, the contribution of 243.17 nm dissociation had to be accounted for in the fit to the velocity distribution by introducing six more parameters (height, width, and position of two Gaussian functions). The contribution of the CCD background signal to the velocity profiles was nonlinear and could be fitted well with a fifth Gaussian function. The resulting I/(I*+I) branching ratios are listed in Table I and are displayed together with previously obtained data in Fig. 3.

TABLE I. Experimental I*/(I*+I) branching ratios. The error in all measurements is below 0.05.

λ(nm)	I*/(I*+I) branching ratios
288	0.122, 0.098
287	0.127, 0.157, 0.155, 0.121
286	0.160
285	0.173, 0.123, 0.136, 0.153
284	0.184, 0.192
283	0.197, 0.192
282	0.257, 0.203, 0.198, 0.240
281	0.219, 0.245
280.2	0.230
280	0.229, 0.231
279	0.277, 0.273
278	0.284
277.92	0.262, 0.265
277	0.301, 0.282
275	0.313, 0.323
274	0.307, 0.310
273	0.321, 0.361, 0.366, 0.330

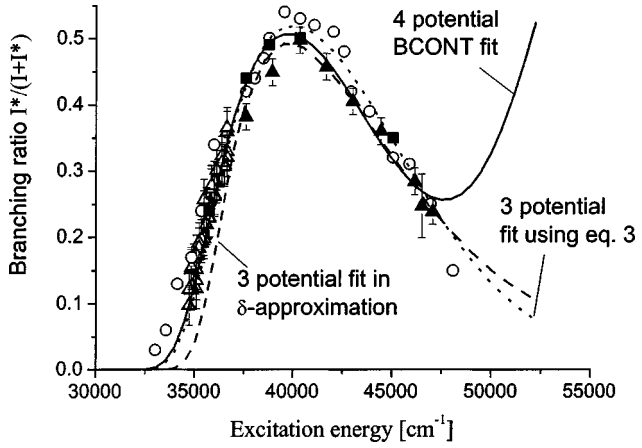

FIG. 3. Experimental and calculated branching ratios. The symbols are: open triangles: BRs from this work; filled triangles: Gendron-Hepburn (Ref. 3); open circles: Langford *et al.* (Ref. 4); and filled squares: Regan *et al.* (Ref. 5). The BR derived from the three potential fit in δ-approximation (long-dashed line), using Eq. (3) (short-dashed line), and the four potential fit with constant $M_u(r)$ from Ref. 7 (solid line) are also shown.

Clearly our data do support previous measurements of the branching ratio and agrees well with both the revised values of RACAO and GH. Our branching ratios have an absolute error of less than 0.05. These errors mainly originate from the fitting of the velocity profiles.

Note that there is a splitting of the contribution from the parallel dissociation channels (the ''polar'' rings) for both the 243 and 277 nm signals. The splitting is equal for both channels—roughly 3 pixels on the CCD image. For the 277 nm channel the splitting corresponds to about 800 m/s of H-atom velocity, i.e., an $\sim$800 cm^{-1} shift in HI ground state energy. As will be shown below, this effect is due to the recoil of protons from the departing electrons. The splitting is too small to be a contribution of vibrationally excited HI parent molecules. Contribution of HI dimers in their lowest vibrational state is plausible, but unlikely since the expansion conditions are such that the formation of dimers and higher clusters is strongly suppressed. Even when the formation of dimers was optimized by Wittig and co-workers[9] or by Young,[10,11] the contribution of HI-dimers to the dissociation signal was well below 10% and nowhere near the $\sim$50% apparent in our ion signal. Also, the ratio of the intensities of these two rings stays roughly the same upon change of the HI concentration in Helium carrier gas from 5% to less than 0.5% and upon change of the stagnation pressure in the molecular beam valve between 2 bar and 0.5 bar. Important is the fact that the splitting is observed only in the pictures obtained using *probe* laser radiation with its polarization aligned perpendicular to the TOF-axis. For example, in Fig. 2 B/D the photofragment image is obtained using parallel polarization of the probe laser, and no splitting is observed.

This effect is caused in the ionization process by the recoil of the protons from the electrons. The 243.17 nm REMPI process of hydrogen atoms results in the release of about 13 700 cm^{-1} of kinetic energy—most of which is carried away by the electron. The proton carries away 1/1824 of the energy, i.e., about 7.5 cm^{-1}. The added velocity for all H atoms is therefore 423 m/s. This velocity corresponds indeed to the observed $\sim$3 pixel splitting of each polar ring. Hydrogen atom recoil in the REMPI detection process is observable in our experiment due to the high resolution of the velocity map imaging setup and has been described in more detail before.[12]

The spatial anisotropy of the photoelectrons and protons is described by a $\cos^2\theta$ distribution, because in the final ionization step a $2s$ electron is ejected into the p continuum. The spatial distribution of the recoiling protons will therefore be aligned parallel to the polarization of the probe laser, which was for all experiments parallel to the polarization of the photolysis laser and therefore perpendicular to the TOF axis. When the 243 nm laser polarization is aligned parallel to the TOF axis, this recoil pattern disappears in the ion image, as can be seen in Figs. 2(B) and 2(D). This effect is present in any experiment using (2+1) REMPI for H atom detection. In the present experiment the signal channels are well separated and the angular distribution can be recovered by integrating over the full, split ring. This is confirmed by the fact that the same anisotropy parameters were found for the well-separated 277 nm ring when the probe laser polarization is parallel to the TOF axis.

ANALYSIS AND FIT TO POTENTIAL ENERGY CURVES

Using the δ-approximation and three exponential potentials

The experimental data can be used for the reconstruction of potential energy curves of the molecule. In early works three[3] or four[2] repulsive states were used to fit the A-band absorption spectrum, with the potential represented by simple exponentials of the form

$$V(R) = \mathrm{A}e^{-\beta(r-r_e)} + C, \tag{1}$$

where r_e is the equilibrium distance of the ground state potential, and C is the appropriate (known) dissociation limit. The commonly used approximations made therein included the so-called δ-approximation, Q-branch and single-J approximations.[13] Also it has been assumed that the transition dipole functions can be treated as constants with respect to the internuclear distance. To estimate the impact of the new BR data presented here on the potential parameters and transition intensities, we used these four assumptions to perform least-squares fitting to the HI total absorption cross section (TACS) by Ogilvie[14] and branching ratios by GH, RACAO, and our new data. The δ-approximation implies that the absorption spectrum is given simply as a function of the excited state potential's gradient[13]

$$\epsilon_T(\upsilon) = \alpha \frac{8\pi^3 10^{-29}}{3hc} \frac{\tilde{\nu}}{g_v} \frac{g_u}{g_l} M_u^2 |(dV/dr|)_{r_0}^{-1} \psi^2(r_v), \tag{2}$$

where $\alpha = 2.6153 \times 10^{-4}$ converts the absorption cross section in $Å^2$ to the extinction coefficient in $mol^{-1}\,cm^{-1}$.[15] Here Planck's constant h, and the speed of light, c, are in SI units, r in Å, M_u in D, and V and $\tilde{\nu}$ in cm^{-1}. The vibrational partition function g_v has been set to unity. The ratio of degeneracies of the upper and the lower states (g_u/g_l) is two for the $\Omega=1$ states and one for the 0^+ state. The slopes of

TABLE II. Potential parameters, transition dipole moments, and estimated total oscillator strengths, *f*, of the three Π states in the A-band of HI. The contribution of the $t\,^3\Sigma_1$ state in the analysis of de Vries *et al.* and Le Roy *et al.* was subtracted out.

State	Parameter	De Vries *et al.*[e,i] Ref. 2	Clear *et al.*[e,j] Ref. 18	G&H[f,i] Ref. 3	This work[i] c, e	This work[i] d, f	Le Roy *et al.*[f,j] Ref. 7
$^1\Pi_1$[a]	A, cm^{-1}	25 890(484)	21 850(350)	24 298(20)	24 129(1510)	23 879(470)	22 143(150)
	β, A^{-1}	2.86(6)	1.90(9)	3.104(8)	3.15(51)	3.15(16)	2.175(60)
	$\langle M_u\rangle^2$, D^2	0.193(25)	0.126(15)	0.003 13(16)	0.240(51)	0.240(16)	0.140(17)
$^3\Pi_1$[a]	A, cm^{-1}	15 808(242)	15 800(250)	11 550(80)	11 306(350)	11 241(109)	16 940(1100)
	β, A^{-1}	2.85(6)	2.85(6)	1.92(3)	2.20(45)	2.16(14)	3.40(27)
	$\langle M_u\rangle^2$, D^2	0.038(4)	0.038(4)	0.000 045(9)	0.0048(9)	0.0049(3)	0.047(17)
$^3\Pi_0$[b]	A, cm^{-1}	12 341(242)	11 250(400)	11 542(13)	11 912(775)	10 882(241)	10 461(190)
	β, A^{-1}	4.8(5)	4.1(1)	3.984(8)	4.07(77)	4.14(24)	4.129(79)
	$\langle M_u\rangle^2$, D^2	0.146(6)	0.160(24)	0.000 77(2)	0.180(39)	0.178(12)	0.164(11)
$^3\Sigma_1$[b]	A, cm^{-1}	12 575(242)					26 479(760)
	β, A^{-1}	3.75(6)	-	-	-	-	2.60 (fixed)
	$\langle M_u\rangle^2$, D^2	0.041(3)					0.143(22)
							11.3[g]
	$1000f$	11.6[g]	9.9[g]			14.4[g]	11.5(7)[b]

[a]C=7603.15 cm^{-1}.
[b]C=0.
[c]$MSR_{BR+TACS}$=5.56%.
[d]$MSR_{BR+TACS}$=1.73%
[e]δ-approximation.
[f]Equation (3).
[g]According to $f\approx 4.7\times 10^{-7} g\langle\nu\rangle\langle M_u\rangle^2$.
[h]The value obtained by integrating the experimental TACS minus the calculated $^3\Sigma_1$ PACS according to $f\approx 4.32\times 10^{-9}\int(\epsilon_\nu\, d\nu)$ (Ref. 13).
[i]HI data only.
[j]Fit to both HI and DI data.

the excited states potential curve dV/dr at the classical turning point r_v are determined by the fitted parameters A and β for each excitation wave number $\tilde{\nu}$.

The nine parameters thus involved are obtained using a home written gradient descent nine-parameter optimization algorithm to minimize the root mean square difference between the original and calculated TACS curves. The wave functions for the HI $v''=0$ ground state function were obtained from the accurate potential energy functions by Coxon and Hajigeorgiou[16] using the analytical formalism by Herman *et al.*[17] A Runge–Kutta expansion was used for the excited state wave function. Two approaches were tested. First, the TACS curve was fitted as a sum of the PACS curves with nine varying parameters. Second, one can make use of the fact that the $^3\Pi(0^+)$ PACS curve can be derived from the TACS and the BR data. Then first only one potential is fitted to the $^3\Pi(0^+)$ PACS curve and the other two to the remainder. This sequential procedure therefore involves not only the TACS but also the experimental branching ratio data of G&H, RACAO, and our work. Since these latter fits are consecutive three and six parameter fits, respectively, the fitting procedure is more robust.

Interestingly, the difference between the TACS and PACS fits was found to be negligible. It should be emphasized that because of the nature of the fitting functions the TACS fit may not converge to the true potential parameter values if the initial values are far off. This was observed when offsetting each of the parameters by 10% and more (>40% in terms of weighted MSR), the dominant states ousting the weak one.

Since the error in the TACS measurement was quoted as being 3%–5%, we weighted the data accordingly. The fit is rigorous, so the resulting error can be considered as stipulated for by the original TACS curve measurement error as well as by the neglect of other possibly contributing states. The results of this fit are given in Table II, and compared to values obtained by Clear *et al.*,[18] de Vries *et al.*[2] and GH. Figure 4(a) shows the decomposition of the absorption spectrum into these three components (dashed lines). When compared to previously published results, our fit using the δ-approximation differs in that the new ''red wing'' BR data further diminish the role of the $^3\Pi(1)$ state. One also notes that the overall convergence is poor, which is especially noticeable in Fig. 3, where the experimental and calculated BRs are shown. This disagreement is a consequence, first, of the δ-approximation not being able to reproduce the ACS shape properly and, second, of the neglected contribution from the higher lying $t\,^3\Sigma_1$ state.

Full quantum simulation with three exponential potentials and flat $M_u(r)$

A more rigorous analysis was then performed based on exact quantum simulations of independent partial cross sections for the participating electronic transitions, calculated using Le Roy's BCONT program.[19] In this approach the

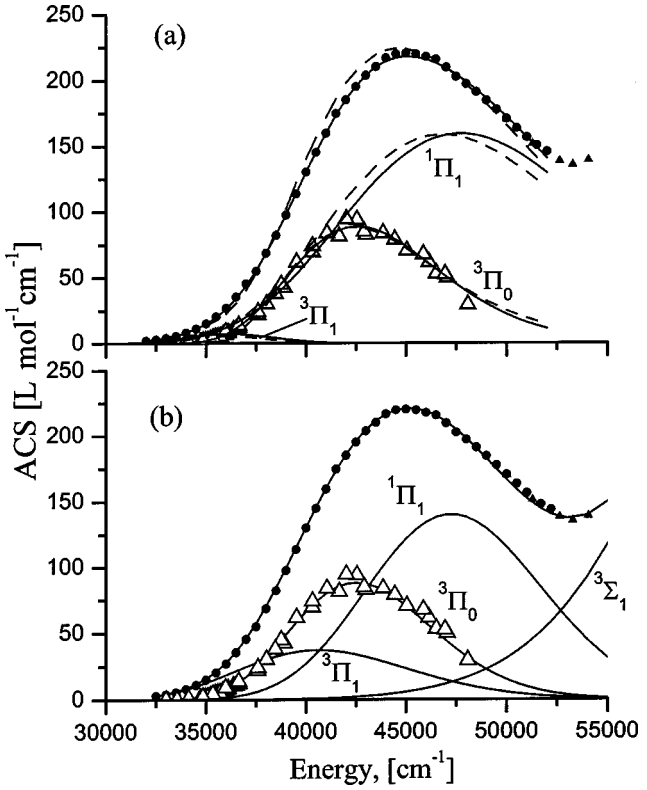

FIG. 4. (a) Total and partial absorption cross-sections of HI from a three potential fit. The dashed curves are obtained in the δ-function approximation, and the solid curves from a fit based on the fully quantum simulation using Eq. (3), both using constant $M_u(r)$ functions. (b) Total and partial quantum-calculated absorption coefficients for HI from the four-state constant-$M_u(r)$ analysis of Ref. 7. For both segments, open triangles are the sum of PACS values of all states that dissociate to form excited I* atomic fragments and are calculated from the TACS and BR data. The filled circles are the experimental absorption data of Ogilvie (Ref. 14); the filled triangles those of Huebert and Martin (Ref. 23).

δ-function approximation was replaced by overlap integrals calculated from exact bound and continuum wave functions, with the partial absorption coefficient for absorption from a thermal initial-state vibration–rotation level population into a given final electronic state being computed from the expression,[7,20]

$$\epsilon_T(\upsilon) = \frac{10^{-9}N_A}{\ln 10}\frac{8\pi^3}{3hc}g\tilde{\upsilon}\sum_{\upsilon}\sum_{J} F_{\upsilon J}(T)\sum_{J'}\frac{S_J^{J'}}{2J+1} \times\left|\int dr\,\psi_{EJ'}(r)M_u(r)\psi_{\upsilon J}(r)\right|^2, \quad (3)$$

where $\tilde{\upsilon}$ is photon energy in cm^{-1}, g the degeneracy, M_u is the transition dipole moment in Debye, υ and J are the initial-state vibrational and rotational quantum numbers, $F_{\upsilon J}(T)$ is the normalized thermal rotation–vibration population distribution function, and J' is the final (continuum) state angular momentum. The functions $\psi_{EJ'}$ and $\psi_{\upsilon J}$ are the unbound and the ground states wave functions, respectively, and $S_J^{J'}$ the Hönl–London rotational intensity factor.

The potential parameters and transition intensities are close to those obtained in the δ-approximation and are listed in Table II. This indicates that a nearby minimum in parameter space has been found. As is shown in Fig. 4(a), the fitted TACS now agrees well with the experimental values, and the branching ratio data is well reproduced.

However, an analogous fit to the DI TACS (not shown) predicts branching ratios which are inconsistent with the available BR data from photofragment imaging measurements[21] and from older photofragment arrival time measurements.[18] Furthermore, the resulting potentials for the two isotopomers did not match well unless the fit was confined to below ca. 47 000 cm^{-1}. This was also noticed by Clear *et al.*[17] who analyzed both HI and DI data and limited their fit to below 48 000 cm^{-1}; whereas de Vries *et al.* introduced the *t* state into the picture.[2]

Finally, when comparing the total oscillator strengths of the three Π states that result from different fits (given in Table II), it is apparent that the data supplied by Clear *et al.* and de Vries *et al.* results in values that are different to the ones we obtain when including the absorption spectrum up to 52 000 cm^{-1}. This is a further indication that the three-state model is inconsistent with the additional data.

From these observations we conclude that not only is the δ-approximation inadequate as a base for understanding the shape of the absorption cross section, but also that even when using the more rigorous quantum model of Eq. (3) one will have to include the contributions of the high-lying $t\,^3\Sigma_1$ state.

At the same time, recent simulations[22] suggest that there is a shallow minimum on the PES for the $^3\Pi_0$ state, so that the previously assumed exponential shape of the potential must be reconsidered. Finally, the same *ab initio* calculations showed that there exists a strong dependence of transition moment functions on internuclear distance. An improved model will have to address these issues properly.

Full quantum simulation with four exponential potentials and flat $M_u(r)$

Taking into account these considerations, our data, which now make up for lack of information on branching ratios in the red region, were used by Le Roy and co-workers[7] to perform a four potential fit using more general expressions for the potential curves, allowing for *r*-dependent transition moment functions, and using rigorous quantum calculations based on Eq. (3).[20] The following paper[7] offers a comprehensive coverage of the possibilities of potential reconstruction based on all spectral and BR data, experimental as well as *ab initio*, for HI and DI, available to date. Here, we only consider those fits that assumed *r*-independent transition dipoles and exponential-wise potentials of the form (1) and therefore allow for direct comparison with previously published potential parameters. Fitting also used the absorption data by Huebert and Martin[23] that go up to 55 000 cm^{-1} and is done simultaneously to data of both HI and DI.

Table II summarizes the constant $M_u(r)$ results by Le Roy and co-workers (not listed explicitly in Ref. 7), while Fig. 4(b) shows the associated predicted decomposition of the HI TACS into PACSs for the four states.[14] As is seen in the figure, the *t* state intensity becomes significant and is much higher than predicted by de Vries.[2] The four-potential

branching ratios are shown as solid curves in Fig. 3, where they are compared with the three-potential δ-function approximation results (short- and long-dashed curves); the former accurately reproduce the experimental measurements except at the very blue end of the spectral region. As shown in Ref. 7, this latter deviation is due to neglect of the r-dependence of the transition moment functions. The small uncertainties in the fitting parameters listed in Table II and the apparent excellent agreement with experimental data for both isotopomers further underlines the necessity of including the fourth potential in the picture, as well as a need for the fully quantum model represented by Eq. (3). This fourth potential modifies the relative contributions of the three lower lying states to the TACS considerably. It also leads to very different potential parameters, which are, due to the nature of the fit, identical for HI and DI.

As expected when comparing the oscillator strengths that result from different fits given in Table II, it is apparent that Le Roy's superior model—after the contribution of the t state has been subtracted out—results in values similar to the ones obtained in the three-state and energy-constricted model used by Clear *et al.* and the four state model by de Vries *et al.*

DISCUSSION

Our branching ratios at the low energy tail of the HI absorption spectrum add further support for both the data obtained by GH and the data by RACAO, in what our branching ratios do not differ by more than about 20% from the previously reported values. We do note, however, that our I*/(I+I*) branching ratios seem to be consistently lower than the ones obtained by RACAO. Because of a better sensitivity of the photofragment imaging technique, we believe our experimental data reliably cover the red wing of the absorption spectrum.

When comparing our fitted parameters to those obtained by GH in a very similar constant $M_u(r)$ analysis,[3] we notice a considerable discrepancy in all potential parameters. We believe the four-potential fit values especially for the lowest lying $^3\Pi_1$ state are more accurate due to the additional data in the red wing of the spectrum. We were not able to explain the large discrepancies of the transition dipoles, however. We note that the M_u values from this study have magnitudes similar to those of Clear *et al.*[18] and de Vries *et al.*,[2] as can be seen from Table II. The differences to the M_u by Clear *et al.* and de Vries *et al.* can be readily explained by the different branching ratio data that those earlier studies had at hand as well as by a less accurate δ-approximation model that was then used, but no explanation for the deviation from GH's value for M_u was apparent to us.

Comparison of the results of three potential versus for potential fits with new BR data presented here clearly show the deficiency of the δ-approximation as well as the necessity of including the t state into the picture.

The quality of the fits confirms that there really exist four dominant states in the A-band region and that the dissociation process is mainly adiabatic with no detectable interactions between the states in the exit channels.

In conclusion, we present improved and extended I*/I branching ratios for the $\Omega=1$ and $\Omega=0$ states of HI in the red wing of the absorption spectrum. It was possible to obtain a more accurate description of the potential energy curves using our data.

ACKNOWLEDGMENTS

S.M. and H.-P.L. thank Dr. Robert Le Roy for many instructive discussions and for providing the results of his calculations to us prior to publication. S.M. is grateful for the hospitality of the Waterloo group and for having been able to work under Dr. Le Roy's instruction.

[1] R. S. Mulliken, Phys. Rev. **51**, 310 (1937).
[2] M. S. de Vries, N. J. A. van Veen, M. Hutchinson, and A. E. de Vries, Chem. Phys. **51**, 159 (1980).
[3] D. J. Gendron and J. W. Hepburn, J. Chem. Phys. **109**, 7205 (1998).
[4] S. R. Langford, P. M. Regan, A. J. Orr-Ewing, and M. N. R. Ashfold, Chem. Phys. **231**, 245 (1998).
[5] P. M. Regan, D. Ascenzi, C. Clementi, M. N. R. Ashfold, and A. J. Orr-Ewing, Chem. Phys. Lett. **315**, 187 (2000).
[6] A. T. J. B. Eppink and D. H. Parker, Rev. Sci. Instrum. **68**, 3477 (1997).
[7] R. J. Le Roy, G. T. Kraemer, and S. Manzhos, J. Chem. Phys. **117**, 9353 (2002) (following paper).
[8] A. T. J. B. Eppink and D. H. Parker, J. Chem. Phys. **110**, 832 (1999).
[9] J. Zhang, M. Dulligan, J. Segall, Y. Wen, and C. Wittig, J. Phys. Chem. **99**, 13680 (1995).
[10] M. A. Young, J. Chem. Phys. **102**, 7925 (1995).
[11] M. A. Young, J. Phys. Chem. **98**, 7790 (1994).
[12] D. H. Parker, R. F. Delmdahl, B. B. L. G. Bakker, and H.-P. Loock, J. Chin. Chem. Soc. (Taipei) **48**, 327 (2001).
[13] R. Schinke, in *Photodissociation Dynamics*, 1st ed. (Cambridge University Press, Cambridge, 1993).
[14] J. F. Ogilvie, Trans. Faraday Soc. **67**, 2205 (1971).
[15] J. Tellinghuisen, in *Photodissociation and Photoionization*, edited by K. P. Lawley (Wiley, Avon, 1985), Vol. LX.
[16] J. A. Coxon and P. G. Hajigeorgiou, J. Mol. Spectrosc. **150**, 1 (1991).
[17] R. M. Herman, R. .H. Tipping, and S. Short, J. Chem. Phys. **53**, 595 (1970).
[18] R. D. Clear, S. J. Riley, and K. R. Wilson. J. Chem. Phys. **63**, 1340 (1975).
[19] R. J. Le Roy and G. T. Kraemer, *BCONT 2.0 Computer Program for Calculating Absorption Coefficients, Emission Intensities or (Golden Rule) Predissociation Rates*, University of Waterloo Chemical Physics Research Report CP-650 (2001). The source code and manual for this program may be obtained from the "Computer Programs" link on the web site *http://leroy.uwaterloo.ca*
[20] R. Le Roy, R. G. Macdonald, and G. Burns, J. Chem. Phys. **65**, 1485 (1976).
[21] L. McDonnell and A. J. R. Heck, J. Mass Spectrom. **33**, 415 (1998).
[22] A. B. Alekseyev, H.-P. Liebermann, D. B. Kokh, and R. J. Buenker, J. Chem. Phys. **113**, 6174 (2000).
[23] B. J. Martin and R. M. Huebert, J. Phys. Chem. **72**, 3046 (1968).